



Single Crystal Growth of Monoisotopic Hexagonal Boron Nitride from a Fe-Cr flux

Journal:	<i>Journal of Materials Chemistry C</i>
Manuscript ID	TC-ART-05-2020-002143.R1
Article Type:	Paper
Date Submitted by the Author:	08-Jun-2020
Complete List of Authors:	Li, Jiahua; Kansas State University Elias, Christine; Université de Montpellier Ye, Gaihua; Texas Tech University System Evans, Dylan; Kansas State University Liu, Song; Kansas State University, Tim Taylor Department of Chemical Engineering He, Rui; Department of Electrical and Computer Engineering, Texas Tech University Cassabois, Guillaume; Laboratoire Charles Coulomb Gil, Bernard; Laboratoire Charles Coulomb Valvin, Pierre ; Université de Montpellier Liu, Bin; Kansas State University, Chemical Engineering Edgar, Jim; Kansas State University, Tim Taylor Department of Chemical Engineering

Single Crystal Growth of Monoisotopic Hexagonal Boron Nitride from a Fe-Cr flux

Jiahan Li¹, Christine Elias², GaihuaYe³, Dylan Evans¹, Song Liu¹, Rui He³, Guillaume Cassabois², Bernard Gil², Pierre Valvin², Bin Liu¹ and James H. Edgar^{1*}

¹Tim Taylor Department of Chemical Engineering, Kansas State University, Manhattan, KS, 66506, United States

²Laboratoire Charles Coulomb (L2C), Université de Montpellier, CNRS, 34095 Montpellier, France

³Department of Electrical and Computer Engineering, Texas Tech University, Lubbock, Texas 79409, United States

E-mail: edgarjh@ksu.edu

Received xxxxxx

Accepted for publication xxxxxx

Published xxxxxx

Abstract

Hexagonal boron nitride (hBN) is an important insulator that is incorporated into numerous 2D electronic, optoelectronic, and photonic devices. Whereas natural hBN is mixture of 20% ¹⁰B and 80% ¹¹B isotopes, monoisotopic hBN is a variant with just a single boron isotope, either ¹⁰B or ¹¹B. Consequently, monoisotopic hBN has a higher thermal conductivity and a stronger neutron absorption (in the case of h¹⁰BN), making it superior for neutron detectors, heat management materials in nano flexible electronic devices, and phonon polariton-based nanophotonics. Here we synthesized approximately monoisotopic hBN using boron powder containing a single boron isotope and nitrogen, and grew single crystals from a Fe-Cr metal flux at atmospheric pressure. Narrow Raman peaks from the shear (≤ 1.3 cm⁻¹) and intralayer (≤ 3.3 cm⁻¹) modes demonstrate that the crystals are highly ordered. In the photoluminescence spectra, the presence of phonon-assistant transition peaks is also indicative of the high-quality of the crystals. This growth protocol permits us to get rid of the emission at 4.1 eV. This work provides a novel material for studies of the fundamental properties of isotope effects and high-performance hBN device.

Keywords: Hexagonal boron nitride, metal flux, monoisotopic hBN, Raman, Photoluminescence

1. Introduction

Hexagonal boron nitride (hBN) has received a lot of attention recently because of its excellent properties such as its chemical inertness, wide energy bandgap (5.9 eV), atomically smooth surface that is free of dangling bonds¹ and high in-plane thermal conductivity². These properties make hBN appealing for such applications as deep UV emitters and detectors,³ substrates and encapsulants for other two-dimensional materials,⁴ quantum emitters,⁵ heat management layers in nano devices, dielectrics,⁶ neutron detectors,⁷ and so on. For these applications, hBN single crystals are needed.

Most current research uses hBN with the natural distribution of boron isotopes: ¹¹B (80.1%) and ¹⁰B (19.9%). Due to the different neutron spin number and atomic masses between the ¹⁰B and ¹¹B isotopes, pure boron and boron compounds with a single isotope (monoisotopic) possess different phonon effects including electron-photon interaction, reduced isotopic disorder and different average isotopic masses.⁸ In the case of hBN, the different properties of ¹⁰B and ¹¹B isotopes affect the corresponding optical excitation spectra and energy gaps.⁹ Monoisotopic boron hBN single crystals are also of interest for investigating the fundamental isotopic effects. The enhanced properties of monoisotopic hBN make it superior for applications in heat management, nanophotonics and thermal neutron detection. For example, because of its anisotropic thermal conductivity (high in-plane and low out-of-plane), chemical stability and mechanical flexibility at high operating temperature, monoisotopic hBN opened up an opportunities for next generation thermal management materials, such as cooling bendable nanoscale microelectronics or thermoelectrics¹⁰. Compared to natural hBN, monoisotopic hBN possesses a higher thermal conductivity because of reduced phonon scattering due to the random distribution of isotopes.^{11, 12} Moreover, while natural abundant hBN crystal is a low-loss phonon polariton material, first-principles calculations predict the polariton lifetimes of monoisotopic hBN is even higher, increased by a factor between four and ten because of less phonon scattering.^{13, 14} Thus, monoisotopic hBN is especially good for realizing high-efficiency, polaritonic devices. A threefold increase in both the bulk phonon lifetimes and propagation length of phonon polariton over the already low-loss natural hBN crystals were experimentally demonstrated.¹³ Furthermore, neutron detectors fabricated with h¹⁰BN epilayers have demonstrated a thermal neutron detection efficiency of 51.4%, which is the highest among all semiconductor neutron detectors.¹⁵

Despite its promise, monoisotopic boron hBN single crystal growth has not been well studied. To the best of our knowledge, h¹¹BN has not been reported by chemical vapor deposition (CVD). h¹⁰BN epitaxy layers were grown by CVD on sapphire substrates, however, they are not single crystalline.¹⁶

Our group has previously reported the single crystal growth of monoisotopic hexagonal boron nitride from Ni-Cr flux.¹⁷ Approximately monoisotopic boron powders, i.e., ¹⁰B (99.22 at.%) and ¹¹B (99.41 at.%), and nitrogen were used as the precursors. Both h¹⁰BN and h¹¹BN single crystals were produced from Ni-Cr flux solvents at 850 torr. Their Raman peak widths were narrow (~ 3 cm⁻¹), indicating their excellent structural quality. There is a clear spectral shift in both shear and intralayer modes in monoisotopic hBN.

Here we test whether an iron-chromium flux is also suitable for growing monoisotopic hBN crystals. For crystals grown by metal flux techniques, impurities can degrade the hBN quality. Potential sources of impurities in the hBN are the metals comprising the flux (Ni, Fe, and Cr), as well as impurities in the metal fluxes (carbon and oxygen for example). These impurities can incorporate either as precipitates (inclusions), substitutionally on lattices sites, or intercalated between the layers of hBN.^{18, 19} Iron is an attractive potential alternative to nickel because it is less expensive and commercially available in high purity. Our prior study demonstrated that Fe-Cr metal flux can grow hBN with the natural boron distribution from a hot pressed boron nitride source.²⁰

In this study, h¹⁰BN and h¹¹BN crystals were grown from a Fe-Cr flux. Crystal growth by this method is complex as it involves the simultaneous reaction of boron and nitrogen to form hBN, the dissolution of solids (boron and boron nitride) and a gas (nitrogen), into the hot solution, and hBN crystal nucleation and growth as the solution is cooled. Consequently, it is difficult or even impossible to predict *a priori* the outcome. Thus, it is necessary to evaluate this process through experiments, and to characterize the properties of the crystals produced. The crystal quality was characterized by optical microscopy, and Raman and photoluminescence spectra.

2. Experimental methods

2.1 Bulk single crystal growth

Approximately monoisotopic boron hBN ($h^{10}\text{BN}$ and $h^{11}\text{BN}$) crystals were grown by the metal flux method, which is schematically illustrated in Figure 1. The high-purity 30g iron shot (4H8 purity, carbon content: 1ppm), 30g chromium granules (5N purity, carbon content 12 ppm) and ^{10}B (99.22 at.%) or ^{11}B (99.41 at.%) powders were mixed and loaded into an alumina crucible which was then put in an alumina tube furnace with single horizontal heating zone. Before heating the furnace, the alumina tube was purged three times by forming gases (95% Ar and 5% H_2) and N_2 , and then filled to a pressure of 820 torr. The flow rate of N_2 and forming gas were 700 and 30 sccm, respectively. The alumina crucible was heated to 1550 °C and held for 24h. During the crystal growth process, boron and nitrogen were dissolved in the Fe-Cr flux. Then the crucible was cooled down to 1450 °C at a cooling rate of 4 °C/h. hBN crystals precipitated during the cooling process. Finally, the furnace was quenched to room temperature at 200 °C /h, causing the metal flux to solidify into a metal ingot. Forming gases and N_2 flow continuously during the experimental process. The solidified metal ingot was covered by $h^{10}\text{BN}$ or $h^{11}\text{BN}$ crystals. In order to characterize the hBN, free-standing flakes were peeled from the metal flux using thermal release tape.

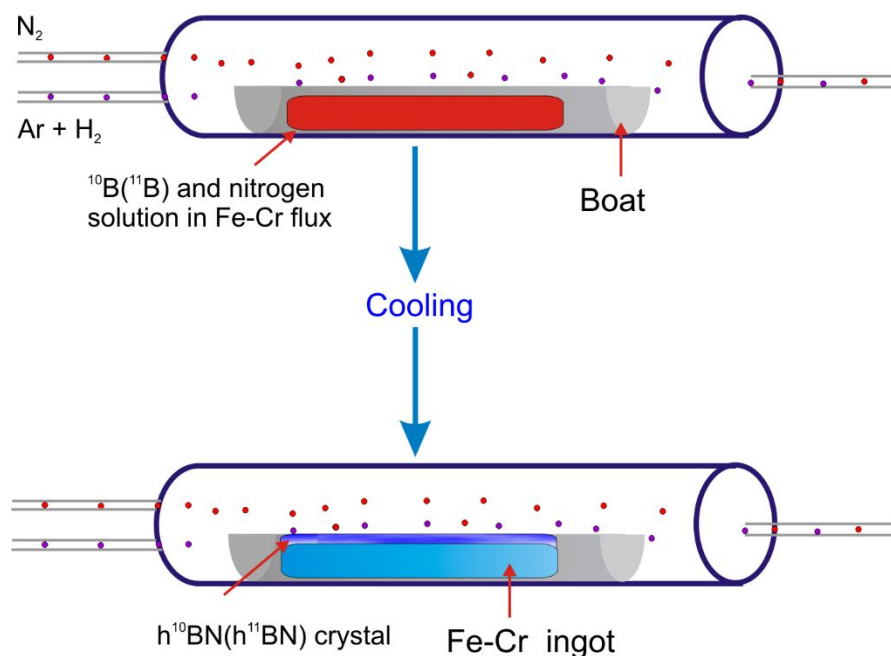


Figure 1. Schematic diagram illustrating the monoisotopic boron hBN crystal growth process. Boron and nitrogen were dissolved in Fe-Cr flux at high temperature (top), then hBN single crystal precipitated on the metal flux surface during cooling process (bottom).

2.2 Raman spectra

Raman spectra were taken at room temperature using a Horiba Labram HR Raman microscope system. A 532 nm laser was used. The laser spot was focused by a 100x lens to a spot diameter of $\sim 1 \mu\text{m}$. By using an 1800 groove/mm grating, we achieved an instrument resolution of $\sim 0.5 \text{ cm}^{-1}$. Raman peaks are well fitted using Lorentzian lineshape.

2.3 Photoluminescence spectra

The opto-electronic properties of the $h^{10}\text{BN}$ and $h^{11}\text{BN}$ single crystals were characterized by PL spectroscopy. The hBN crystals were mounted on the cold finger of a closed-cycle cryostat at a temperature of 10K. The excitation beam is the fourth harmonic of a cw mode-locked Ti-Sa oscillator (194 nm) with a repetition frequency of 82 MHz. The beam was focused on the sample with a spot diameter of $\sim 50\mu\text{m}$ and a power of $\sim 35\mu\text{W}$. An achromatic optical system couples the emitted signal to the detection system using parabolic mirrors with a special coating for deep UV. The detection system was composed of a $f = 300\text{ mm}$ Czerny-Turner monochromator, equipped with a 1800 grooves/mm grating blazed at 250 nm, and a back-illuminated CCD camera (Andor Newton 920), with a quantum efficiency of 50% at 210 nm, operated over integration times of 1 min.

3. Results and Discussion

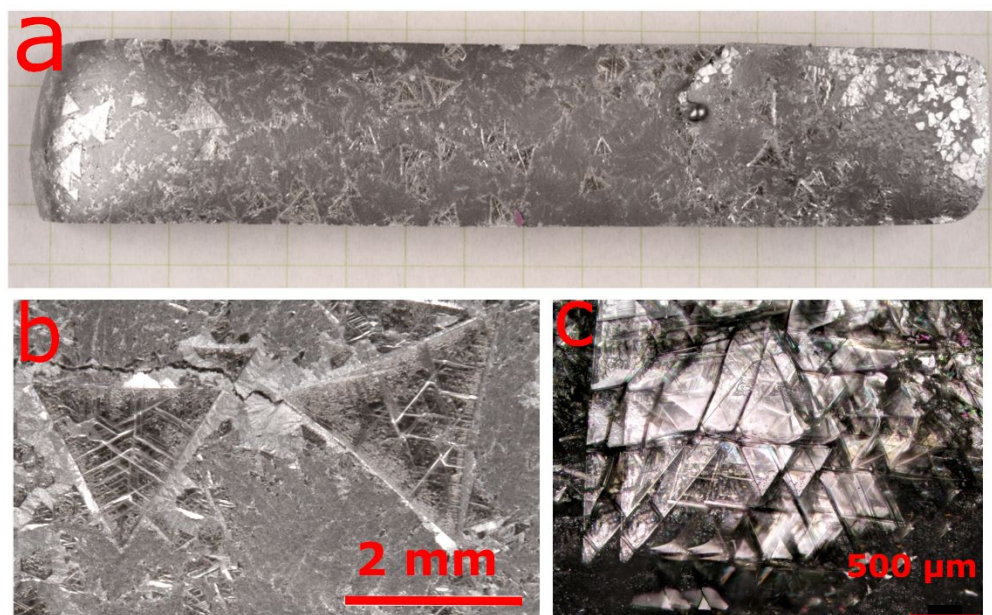


Figure 2. (a) Single crystals of $h^{11}\text{BN}$ on the top surface of the Fe-Cr ingot. The grid size $5\text{ mm} \times 5\text{ mm}$. (b) An enlarged region of the $h^{11}\text{BN}$ crystal grown from Fe-Cr on the top surface of ingot. (c) Micro images of $h^{11}\text{BN}$ crystals grown from Fe-Cr.

Figure 2a is a macro image, showing an example of $h^{11}\text{BN}$ crystals on the Fe-Cr ingot. Some individual triangular and imperfect polygonal shapes formed on the top surface of the Fe-Cr ingot, which is the typical morphology of hBN grown from a metal flux.^{17, 20, 21} There were some opaque areas on the surface of ingot (Figure 2b), which comes from small size $h^{11}\text{BN}$ crystal due to the high supersaturation during nucleation process. The domain size was as large as 5 mm across, presumably indicating low nucleation density in this area during the crystal growth process.

To better understand the surface morphology, the ingot was examined by optical microscopy (Figure 2c). Some domains overlap each other, like fish scales. The crystals were highly transparent and colorless. The Fe-Cr alloy can be seen through the transparent hBN crystals. The entire surface was not fully covered by $h^{11}\text{BN}$ crystal: bare metal was exposed in some regions. Considering that nitrogen is the only volatile element in the system, this is presumably due to the deficiency of nitrogen during $h^{11}\text{BN}$ crystal precipitation process. Triangles were the predominant crystal shape. The geometric shape of the domain suggests all grains it contain have a similar orientation.

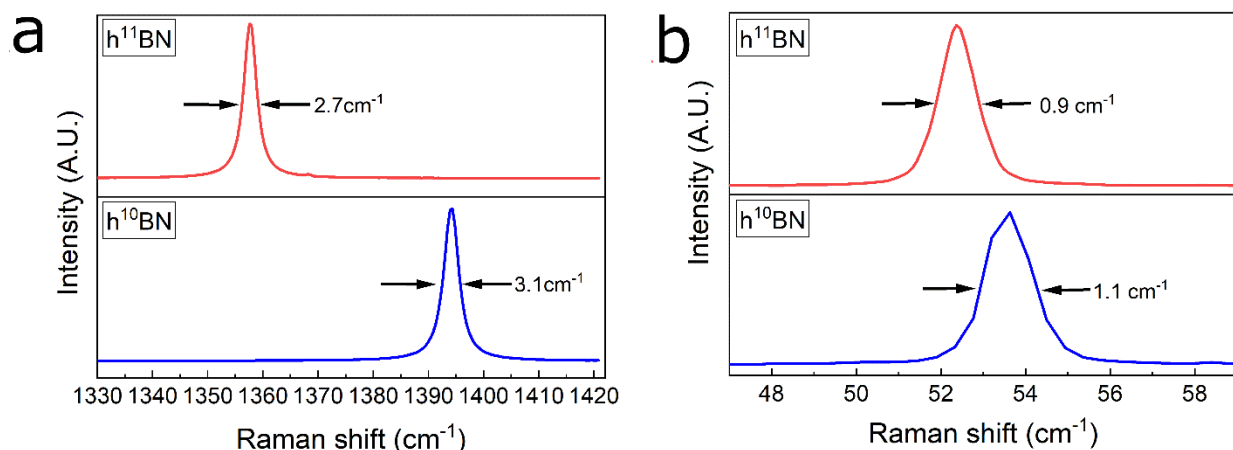


Figure 3. Raman spectra of monoisotopic hBN flakes. (a) Intralayer mode and (b) shear mode.

Figure 3 shows the Raman spectra from $h^{10}\text{BN}$ and $h^{11}\text{BN}$ crystals. Both $h^{10}\text{BN}$ and $h^{11}\text{BN}$ exhibit high (Figure 3a) and low frequency peaks (Figure 3b). The mode at high frequency originates from the intralayer E_{2g} phonon vibration. In contrast, the mode at low frequency is attributed to a vibrational interlayer shear mode, specific to the lateral displacement of atomic layers.²² The peaks of intralayer mode in $h^{10}\text{BN}$ and $h^{11}\text{BN}$ are at 1394.2 cm^{-1} and 1357.7 cm^{-1} , respectively. The full-width-at-half-maximum (FWHM) values for $h^{10}\text{BN}$ and $h^{11}\text{BN}$ are 3.1 and 2.7 cm^{-1} . Both are comparable to that from $h^{10}\text{BN}$ and $h^{11}\text{BN}$ grown from Ni-Cr (3.1 and 3.3 cm^{-1} , respectively)¹⁷, which suggests that the $h^{10}\text{BN}$ and $h^{11}\text{BN}$ crystals are highly crystalline with quality comparable to our monoisotopic hBN grown from Ni-Cr flux.

The E_{2g} phonon energy from $h^{10}\text{BN}$ is higher than that from $h^{11}\text{BN}$. The ratio of observed E_{2g} phonon frequency $\omega_{h^{10}\text{BN}}/\omega_{h^{11}\text{BN}}=1.027$. This is due to the boron atomic mass difference of ^{10}B and ^{11}B . In a harmonic oscillator model, the vibrational frequency of a binary atoms lattice is proportional to $\sqrt{\frac{1}{m_B} + \frac{1}{m_N}}$, m_B and m_N are atomic mass of boron and nitrogen atoms, respectively.²³ From the masses of ^{10}B , ^{11}B and N atoms, we can estimate that the vibrational frequency ratio $\omega_{h^{10}\text{BN}}/\omega_{h^{11}\text{BN}}=1.028$, which agrees with our observed Raman frequency ratio. The FWHM values of both $h^{10}\text{BN}$ and $h^{11}\text{BN}$ are much smaller than that from natural abundant hBN (7.8 cm^{-1})¹⁷, which is attributed to the isotopic disorder effect in natural hBN. Isotopic mass fluctuation interrupts the translational symmetry of isotopically pure atoms and causes elastic scattering of phonons. Therefore, monoisotopic hBN without isotopic mass fluctuation has less elastic scattering of phonons⁸.

The low frequency peak of $h^{10}\text{BN}$ and $h^{11}\text{BN}$ appears at 53.6 (FWHM of 0.9 cm^{-1}) and 52.4 (FWHM of 1.1 cm^{-1}) cm^{-1} , respectively. The FWHM values of this Raman peak from both $h^{11}\text{BN}$ and $h^{10}\text{BN}$ are slightly smaller than monoisotopic hBN grown from Ni-Cr flux (1.3 cm^{-1})¹⁷, which indicates that both $h^{11}\text{BN}$ and $h^{10}\text{BN}$ grown from Fe-Cr flux may have less stacking defects than Ni-Cr. Similar to the intralayer E_{2g} mode, for $h^{10}\text{BN}$, the shear mode exhibits a blue shift in comparison to $h^{11}\text{BN}$. The phonon energy difference is also attributed to the mass difference of ^{10}B and ^{11}B .

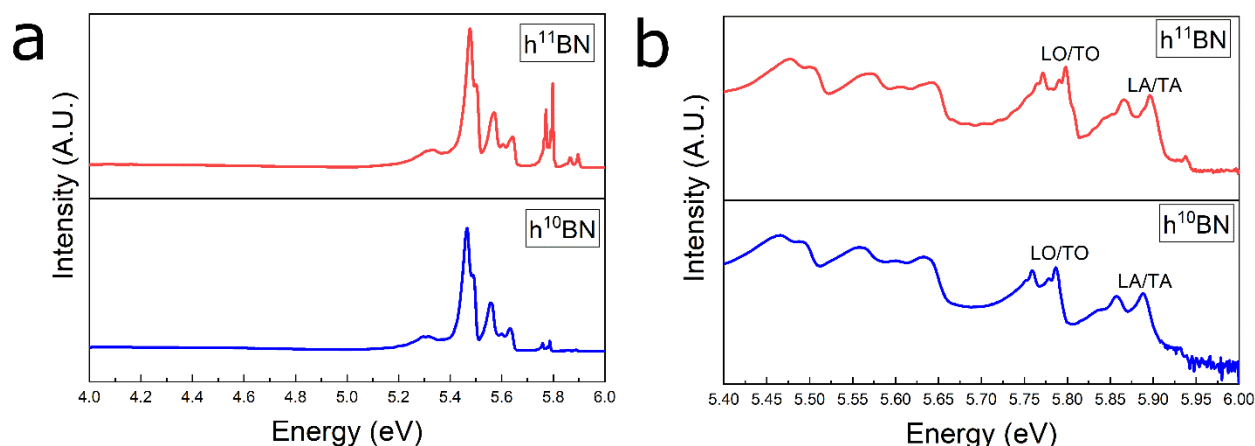


Figure 4. (a) Photoluminescence (PL) spectra of $h^{10}\text{BN}$ and $h^{11}\text{BN}$ at 8K. (b) PL spectra of $h^{10}\text{BN}$ and $h^{11}\text{BN}$ on a log scale ranging from 5.0 eV to 6.0 eV.

Figure 4 demonstrates photoluminescence spectra of $h^{10}\text{BN}$ and $h^{11}\text{BN}$ crystals. As Figure 4a illustrates, there are no emission peaks around 4.1 eV, indicating low concentration of carbon, oxygen impurities and other point defects.^{24,25} These sharp peaks at 4.1 eV are correlated to the impurities in the source materials and it was in particular emphasized that they can be detected in the BN powder used for the growth.²⁴ Here, in contrast to growth protocols involving a hot pressed boron nitride source,²⁰ the using of monoisotopic boron powders, i.e., ^{10}B and ^{11}B , and nitrogen as the precursors loaded into an alumina crucible that was put in an alumina tube furnace leads to samples free from emission at these energies. This rules out that oxygen dissolves from alumina crucible as a contaminant. Because hBN is an indirect semiconductor, radiative recombination must be assisted by the emission of phonons to conserve the energy and momentum. Consequently, the PL spectra of hBN is composed of many phonon replica lines, which is attributed to the different paths of phonon emission.²⁶⁻²⁸ Figure 4b shows PL spectra of monoisotopic hBN ranging from 5.4 eV to 6.0 eV. The lines between 5.4 and 5.7 eV are known as the D lines, which come from inter-K valley scattering assisted by phonons at the K point of the Brillouin zone. The stacking defects of bulk crystals provide density of states and make the inter-K valley scattering observable.²⁸ The four peaks between 5.75 and 5.90 eV correspond to radiative recombination assisted by the emission of phonons, specifically longitudinal optical (LO), transverse optical (TO), longitudinal acoustic (LA) and transverse acoustic (TA) phonons, respectively. The presence of those sharp and intense peaks indicate the crystal have better crystallinity and fewer impurities and defects than many previous studies in which that the peaks were not observed.²⁹⁻³¹ We note the PL spectrum is globally slight blueshift in $h^{11}\text{BN}$, compared to $h^{10}\text{BN}$. From Raman spectra (Figure 3), we confirmed that the phonon energy of $h^{11}\text{BN}$ is smaller than $h^{10}\text{BN}$. The lower the phonon energy, the lower the energy detuning with the indirect bandgap.^{8,26} Therefore, the energy of the phonon replica of $h^{10}\text{BN}$ is lower than $h^{11}\text{BN}$.

4. Conclusions

In summary, we successfully synthesized monoisotopic boron hBN bulk single crystals from Fe-Cr flux, which is significantly cheaper and more pure than Ni-Cr flux. The small FWHM values of shear mode and intralayer mode in Raman spectra demonstrate the crystal quality is comparable to the $h^{10}\text{BN}$ and $h^{11}\text{BN}$ grown from Ni-Cr flux. Phonon-assisted transitions in photoluminescence (PL) spectra caused by longitudinal optical (LO) and transverse optical (TO), longitudinal acoustic (LA), transverse acoustic (TA) phonons confirm that the crystals are the high quality, with few defects and impurities. These $h^{10}\text{BN}$ and $h^{11}\text{BN}$ crystals are useful for investigating the isotopic effects on the electronic and optical properties, and for devices incorporating hBN.

Acknowledgements

Support from the Materials Engineering and Processing program of the National Science Foundation, Award Number CMMI 1538127, and the II–VI Foundation is greatly appreciated. Work at TTU is supported by NSF CAREER Grant No. DMR-1760668. This work was financially supported in France by the contract BONASPES (ANR-19-CE30-0007-02) under the umbrella of the publicly funded Investissements d’Avenir program managed by the French ANR agency.

References

- (1) Heilmann, M., Bashouti, M., Riechert, H.; Lopes, J. Defect mediated van der Waals epitaxy of hexagonal boron nitride on graphene. *2D Materials* **2018**, *5*, 025004.
- (2) Zheng, J., Zhang, L., Kretinin, A. V., Morozov, S. V., Wang, Y. B., Wang, T., Li, X., Ren, F., Zhang, J.; Lu, C. High thermal conductivity of hexagonal boron nitride laminates. *2D Materials* **2016**, *3*, 011004.
- (3) Ahmed, K., Dahal, R., Weltz, A., Lu, J., Danon, Y.; Bhat, I. Growth of hexagonal boron nitride on (111) Si for deep UV photonics and thermal neutron detection. *Appl. Phys. Lett.* **2016**, *109*, 113501.
- (4) Wang, X., Hossain, M., Wei, Z.; Xie, L. Growth of two-dimensional materials on hexagonal boron nitride (h-BN). *Nanotechnology* **2018**, *30*, 034003.
- (5) Schell, A. W., Svedendahl, M.; Quidant, R. Quantum Emitters in Hexagonal Boron Nitride Have Spectrally Tunable Quantum Efficiency. *Adv Mater* **2018**, *30*, 1704237.
- (6) Movva, H. C., Rai, A., Kang, S., Kim, K., Fallahzad, B., Taniguchi, T., Watanabe, K., Tutuc, E.; Banerjee, S. K. High-mobility holes in dual-gated WSe₂ field-effect transistors. *ACS nano* **2015**, *9*, 10402.
- (7) Li, J., Dahal, R., Majety, S., Lin, J.; Jiang, H. Hexagonal boron nitride epitaxial layers as neutron detector materials. *Nuclear Instruments and Methods in Physics Research Section A: Accelerators, Spectrometers, Detectors and Associated Equipment* **2011**, *654*, 417.
- (8) Vuong, T., Liu, S., Van der Lee, A., Cuscó, R., Artús, L., Michel, T., Valvin, P., Edgar, J., Cassabois, G.; Gil, B. Isotope engineering of van der Waals interactions in hexagonal boron nitride. *Nature materials* **2018**, *17*, 152.
- (9) Cardona, M.; Thewalt, M. Isotope effects on the optical spectra of semiconductors. *Reviews of modern physics* **2005**, *77*, 1173.
- (10) Akinwande, D., Petrone, N.; Hone, J. Two-dimensional flexible nanoelectronics. *Nature communications* **2014**, *5*, 5678.
- (11) Lindsay, L., Broido, D.; Reinecke, T. Phonon-isotope scattering and thermal conductivity in materials with a large isotope effect: A first-principles study. *Physical Review B* **2013**, *88*, 144306.
- (12) Yuan, C., Li, J., Lindsay, L., Cherns, D., Pomeroy, J. W., Liu, S., Edgar, J. H.; Kuball, M. Modulating the thermal conductivity in hexagonal boron nitride via controlled boron isotope concentration. *Communications Physics* **2019**, *2*, 43.
- (13) Giles, A. J., Dai, S., Vurgaftman, I., Hoffman, T., Liu, S., Lindsay, L., Ellis, C. T., Assefa, N., Chatzakis, I.; Reinecke, T. L. Ultralow-loss polaritons in isotopically pure boron nitride. *Nature materials* **2018**, *17*, 134.
- (14) Cuscó, R., Edgar, J., Liu, S., Cassabois, G., Gil, B.; Artús, L. Effects of isotopic substitution on the phonons of van der Waals crystals: the case of hexagonal boron nitride. *J. Phys. D* **2019**, *52*, 303001.
- (15) Maity, A., Doan, T., Li, J., Lin, J.; Jiang, H. Realization of highly efficient hexagonal boron nitride neutron detectors. *Appl. Phys. Lett.* **2016**, *109*, 072101.
- (16) Maity, A., Grenadier, S., Li, J., Lin, J.; Jiang, H. Toward achieving flexible and high sensitivity hexagonal boron nitride neutron detectors. *Appl. Phys. Lett.* **2017**, *111*, 033507.
- (17) Liu, S., He, R., Xue, L., Li, J., Liu, B.; Edgar, J. H. Single Crystal Growth of Millimeter-Sized Monoisotopic Hexagonal Boron Nitride. *Chemistry of Materials* **2018**, *30*, 6222.
- (18) Bugaris, D. E.; zur Loye, H. Materials discovery by flux crystal growth: quaternary and higher order oxides. *Angewandte Chemie International Edition* **2012**, *51*, 3780.
- (19) Canfield, P. C.; Fisk, Z. Growth of single crystals from metallic fluxes. *Philos. Mag. B* **1992**, *65*, 1117.
- (20) Liu, S., He, R., Ye, Z., Du, X., Lin, J., Jiang, H., Liu, B.; Edgar, J. H. Large-Scale Growth of High-Quality Hexagonal Boron Nitride Crystals at Atmospheric Pressure from an Fe–Cr Flux. *Crystal Growth & Design* **2017**, *17*, 4932.
- (21) Liu, S., Van Duin, A. C., Van Duin, D. M., Liu, B.; Edgar, J. H. Atomistic insights into nucleation and formation of hexagonal boron nitride on nickel from first-principles-based reactive molecular dynamics simulations. *ACS nano* **2017**, *11*, 3585.

- (22) Stenger, I., Schue, L., Boukhicha, M., Berini, B., Placais, B., Loiseau, A.; Barjon, J. Low frequency Raman spectroscopy of few-atomic-layer thick hBN crystals. *2D Materials* **2017**, *4*, 031003.
- (23) Perkowitz, S. *Optical characterization of semiconductors: infrared, Raman, and photoluminescence spectroscopy*; Elsevier: 2012.
- (24) Pelini, T., Elias, C., Page, R., Xue, L., Liu, S., Li, J., Edgar, J., Dréau, A., Jacques, V.; Valvin, P. Shallow and deep levels in carbon-doped hexagonal boron nitride crystals. *Physical Review Materials* **2019**, *3*, 094001.
- (25) Vuong, T., Cassabois, G., Valvin, P., Ouerghi, A., Chassagneux, Y., Voisin, C.; Gil, B. Phonon-photon mapping in a color center in hexagonal boron nitride. *Phys. Rev. Lett.* **2016**, *117*, 097402.
- (26) Cassabois, G., Valvin, P.; Gil, B. Hexagonal boron nitride is an indirect bandgap semiconductor. *Nature Photonics* **2016**,
- (27) Vuong, T., Cassabois, G., Valvin, P., Jacques, V., Cuscó, R., Artús, L.; Gil, B. Overtones of interlayer shear modes in the phonon-assisted emission spectrum of hexagonal boron nitride. *Physical Review B* **2017**, *95*, 045207.
- (28) Cassabois, G., Valvin, P.; Gil, B. Intervalley scattering in hexagonal boron nitride. *Physical Review B* **2016**, *93*, 035207.
- (29) Majety, S., Cao, X., Li, J., Dahal, R., Lin, J.; Jiang, H. Band-edge transitions in hexagonal boron nitride epilayers. *Appl. Phys. Lett.* **2012**, *101*, 051110.
- (30) Vuong, T., Cassabois, G., Valvin, P., Jacques, V., Van Der Lee, A., Zobelli, A., Watanabe, K., Taniguchi, T.; Gil, B. Phonon symmetries in hexagonal boron nitride probed by incoherent light emission. *2D Materials* **2016**, *4*, 011004.
- (31) Li, J., Cao, X., Hoffman, T. B., Edgar, J. H., Lin, J.; Jiang, H. Nature of exciton transitions in hexagonal boron nitride. *Appl. Phys. Lett.* **2016**, *108*, 122101.